

## Supplementary Information

# Tuning the activity and selectivity of polymerised ionic liquid-stabilised ruthenium nanoparticles through anion exchange reactions

Dambarudhar Parida,<sup>1,2</sup> Camille Bakkali-Hassani,<sup>1</sup> Eric Lebraud,<sup>3</sup> Christophe Schatz,<sup>1</sup> Stéphane Grelier,<sup>1</sup> Daniel Taton,<sup>1</sup> Joan Vignolle<sup>1\*</sup>

<sup>1</sup>Laboratoire de Chimie des Polymères Organiques (LCPO), University of Bordeaux, F-33607 Pessac Cedex, France

<sup>2</sup>Swiss Federal Laboratories for Materials Science and Technology (Empa), CH-9014, St. Gallen, Switzerland

<sup>3</sup>University of Bordeaux, ICMCB, UPR 9048, F-33600 Pessac, France

### Corresponding Author

Joan Vignolle

E-mail: joan.vignolle@enscbp.fr

## Table of Contents

---

<b>1. Materials</b>	<b>3</b>
<b>2. General procedures</b>	<b>3</b>
<b>3. Ru content determination by TGA</b>	<b>7</b>
<b>4. TEM Analysis of Ru nanoparticles</b>	<b>9</b>
<b>5. X-ray diffraction (XRD) patterns of Ru NPs</b>	<b>11</b>
<b>6. <math>\zeta</math>-potentials of Ru NPs</b>	<b>13</b>
<b>7. XPS analysis</b>	<b>14</b>
<b>8. Catalytic activity</b>	<b>24</b>
<b>9. Activity switching of Ru NPs</b>	<b>26</b>
<b>10. References</b>	<b>27</b>

---

## 1. Materials

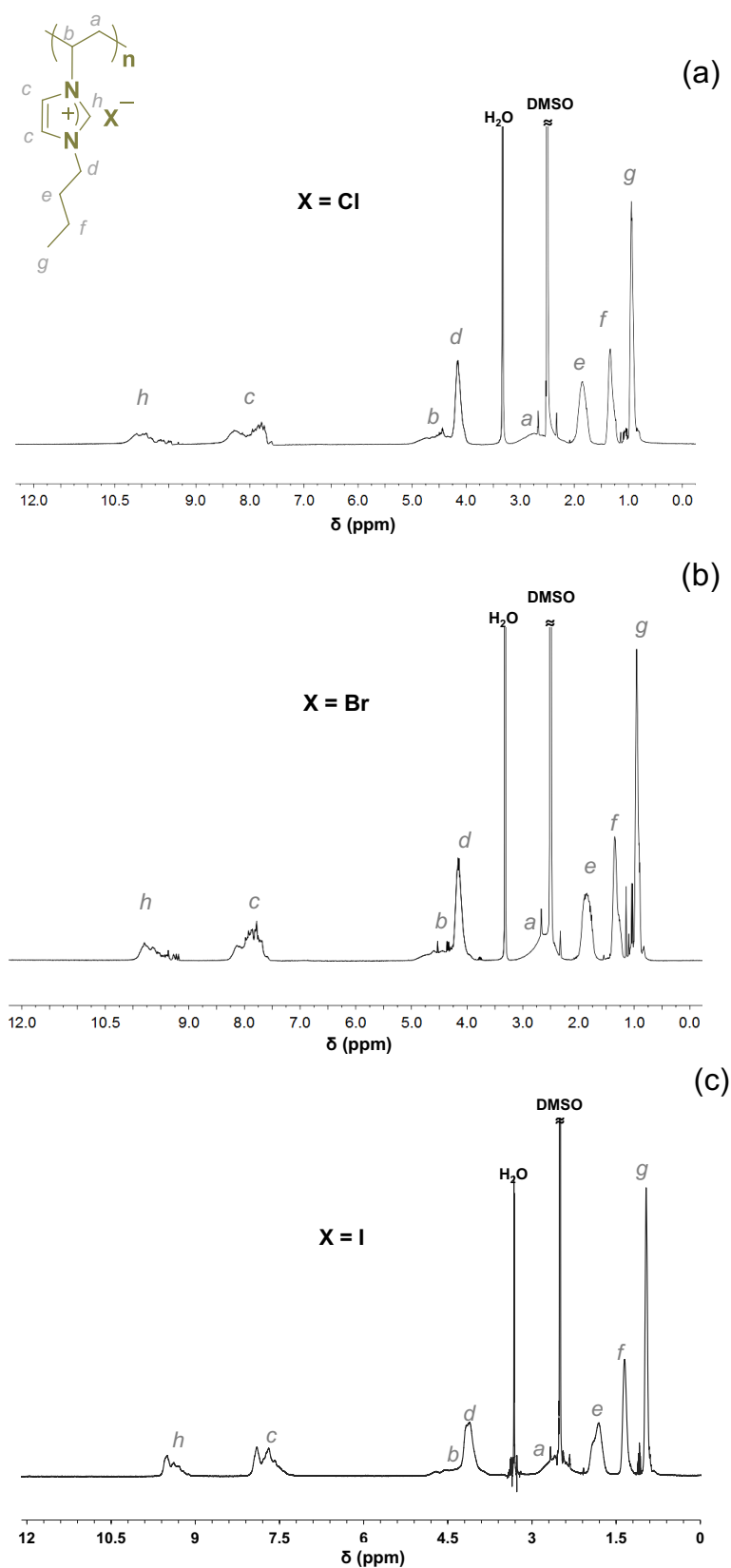
1-Vinyl-3-imidazolium, 1-chlorobutane, 1-bromobutane, 1-iodobutane, and Poly(vinylpyrrolidone) (MW 55000 g/mol) (PVP) were purchased from Sigma Aldrich, France. Ruthenium chloride hydrate (99.9%) and ruthenium bromide hydrate (99.9%) were purchased from Strem Chemicals. Lithium bis(trifluoromethanesulfonimide) (LiNTf<sub>2</sub>) was purchased from TCI France. Ru on Carbon (Ru/C 5%) was purchased from Alfa Aesar France and used as received. HPLC grade solvents were used for synthesis, purification and analysis. All reagents and solvents were used without further purification unless otherwise mentioned.

## 2. General procedures

### (a) Synthesis of Ionic liquids (monomers) and Polyionic liquids

1-butyl-3-vinylimidazolium halides (Cl, Br and I) were synthesized following methods reported in the literature.<sup>1,2</sup> NMR data match those reported in the literature.<sup>1-3</sup> Polymerizations of ionic liquids (ILs) were carried out in isopropanol at 70 °C for 24 hours using azobis(2-methylpropionitrile) (AIBN) as thermal initiator. In all cases molar ratio between IL and AIBN was 200 and polymerization was carried out under an inert atmosphere. <sup>1</sup>H NMR analysis after polymerization confirmed 100% conversion of IL(Cl) and IL(Br). Conversion of 75% was obtained in the case of IL(I) after 48 hours of polymerization. Poly(1-butyl-3-vinylimidazolium chloride) (PIL(Cl)) and Poly(1-butyl-3-vinylimidazolium bromide) (PIL(Br)) were precipitated repeatedly in diethyl ether and dried under vacuum (35 °C) till a constant weight was obtained (quantitative yields). PIL(I) was precipitated once in diethyl ether and then taken for dialysis in methanol to remove the remaining IL(I) monomer. After 48 hours of dialysis, PIL(I) was collected by precipitation in diethyl ether and dried under vacuum (35 °C) till a constant weight was obtained with a yield of 60%. Finally, PILs were analyzed by <sup>1</sup>H NMR to confirm the absence of any unreacted monomers, and <sup>1</sup>H NMR spectra of PIL(Cl), PIL(Br), and PIL(I) are given in Figure S1.

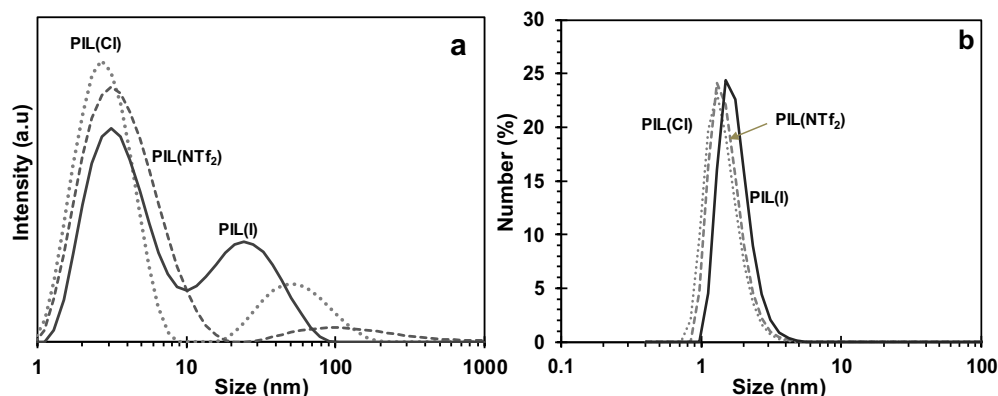
Molecular weight and polydispersity index of PILs were determined by the procedure reported by Matyjaszewski et. al.<sup>4</sup> A GPC system equipped with PSS SDV Linear S (5 μm) column was used at eluent flow-rate of 1 ml/minute. THF containing 10 mmol/L of LiNTf<sub>2</sub> was used as eluent. A viscometer, a multi-angle light scattering detector, and a RI detector from Wyatt Technology were used to acquire elution traces. ASTRA 6.1 software was used for the processing of elution traces. Macromolecular characteristics of different PILs are given in Table S1. For GPC sample preparation anion exchange was carried out on all synthesized PILs to achieve bis(trifluoromethyl)sulfonimide (NTf<sub>2</sub>) anion. Typically, 4 molar equivalent LiNTf<sub>2</sub> dissolved in water (10 ml) was added to a 20 ml aqueous solution of PIL(X) (X is Cl or Br) (10 mg/ml) under stirring. The mixture was stirred for 24 hours to ensure a complete exchange of halide anions (Cl<sup>-</sup> or Br<sup>-</sup>) by NTf<sub>2</sub><sup>-</sup>. Then the precipitate was washed several times with distilled water to remove LiBr and excess LiNTf<sub>2</sub>. The product was then dissolved in acetone, precipitated in water, and centrifuged. PIL(NTf<sub>2</sub>) obtained was dried under vacuum (35 °C) till a constant weight was obtained (quantitative yield). For anion exchange on PIL(I), AgNTf<sub>2</sub> was used instead of LiNTf<sub>2</sub>. In this case, 2 molar equivalent AgNTf<sub>2</sub> dissolved in methanol (10 ml) was added to 20 ml methanol solution of PIL(I) (10 mg/ml) under stirring. After 24 hours, the mixture was centrifuged at 8000 rpm for 15 minutes to remove insoluble AgI. Then, the solution was concentrated by evaporation of methanol and the polymer was recovered by precipitation in water. To ensure complete removal of AgNTf<sub>2</sub>, PIL was precipitated twice in water. Finally, it was dried under vacuum (35 °C) till a constant weight was obtained.



**Figure S1.**  $^1\text{H}$  NMR spectra of (a) Poly(1-vinyl-3-butylimidazolium chloride) (PIL(Cl)) and (b) PIL(Br) and (c) PIL(I). Traces of iso-propanol (from the synthesis) appearing at 1.04 ppm are visible.

**Table S1.** Molecular weight (Mw and Mn) and polydispersity index (PDI) of synthesized PILs.

Entries	Sample	Mw (g/mol)	Mn (g/mol)	PDI
1	PIL(Cl)	59760	33200	1.8
2	PIL(Br)	72576	34560	2.1
3	PIL(I)	59280	45600	1.3
4	PVP	55000 (Sigma)	-	-

**Figure S2.** DLS size of PIL(Cl), PIL(NTf<sub>2</sub>) and PIL(I) shown in (a) intensity-average and (b) number average. DLS experiment was carried out at 25 °C using methanol as the common solvent for PILs.**(b) Preparation of Ru nanoparticles**

RuCl<sub>3</sub>·xH<sub>2</sub>O and RuBr<sub>3</sub>·xH<sub>2</sub>O were used as metal precursors and PIL(Cl), PIL(Br) or PIL(I) as stabilizers for the synthesis of PIL(X)-stabilized Ru nanoparticles (NPs) (X = Cl, Br, I). The different molar ratio between PIL(X) (IL(X) units) to metal salt (i.e. 50:1, 10:1, 2:1) were used to synthesize PIL(X)@Ru NPs, namely **1-3Cl**, **2Br** and **2I** via polyol process.<sup>5,6</sup> Typically, 400 mg of PIL(X) and the required quantity of metal salt were dissolved in 40 ml ethylene glycol in a 200 ml schlenk flask. After stirring for 4 hours at 750 rpm, the resulting dark yellow solution was degassed with argon and immersed in an oil bath preheated at 170 °C. The dark yellow solution slowly turned black, indicating the formation of Ru(0)NPs. Heating was continued for 1.5 hours to ensure complete conversion of ruthenium salt to Ru(0) and formation of NPs which was confirmed by UV-vis spectroscopy analysis. The disappearance of the broad absorption band in the spectrum of the precursor after reduction indicates complete reduction of Ru(+2) into Ru(0). A representative example is given in Figure S3 with the reduction of RuCl<sub>3</sub> in presence of PIL(Cl). PILs stabilized NPs were collected by centrifuging 5 ml of NP solution with 30 ml of a mixture of diethyl ether and acetone (50:50). After this initial centrifugation, RuNPs were dissolved in acetone (15 ml) and diethyl ether was added (20 ml); the resulting suspension was then subjected to centrifugation. This step was repeated one more time. The resulting sticky black product was next dissolved in 5 ml of methanol and centrifuged with 25 ml of diethyl ether. All centrifugations were carried out at 8000 rpm for 15 min at 15 °C. The resulting shiny black product was vacuum (0.8 mmHg) dried at 35 °C till a constant weight was obtained (24 - 48h). This step ensures the removing of the different solvents, including ethylene glycol (b.p. = 197°C). The same procedure was followed for the preparation of PVP-stabilized RuNPs and 1-Butyl-3-methylimidazolium bromide-stabilized RuNPs.

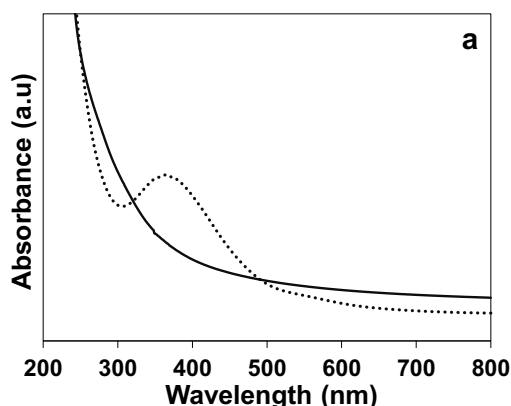


**Figure S3.** UV-Vis spectra of precursor solution ( $\text{RuCl}_3 + \text{PIL}(\text{Cl})$ ) showing the characteristic absorption band (dotted line) of  $\text{RuCl}_3$  around 365 nm and diffused absorption band was observed after reduction (solid line). Diffused absorption indicates the complete reduction of  $\text{RuCl}_3$  and formation of very small Ru nanoparticles.<sup>7,8</sup>

**(c) Anion exchange on PILs stabilized Ru NPs**

**Anion exchange via  $\text{LiNTf}_2$ :** To change the solubility and study the effect of anion on the catalytic activity of Ru NPs, anion exchange was carried out on **2Br**. In a typical anion exchange reaction, 10 ml aqueous solution of  $\text{LiNTf}_2$  (4 molar equivalent) was added dropwise to 30 ml aqueous solution (1.5 mg/ml) of **2Br** under vigorous stirring, leading to the slow precipitation of **2NTf<sub>2</sub>**. To ensure complete anion exchange, the mixture was stirred for 16 hours under ambient temperature (see also XPS data in Figures S14 and S15). All operations were carried out under an argon atmosphere. The resulting precipitates were washed several times with water and then dried under vacuum at 35 °C till a constant weight was obtained. After anion exchange, NPs became hydrophobic and soluble in organic solvents, as given in the solubility chart (Table S1). The same procedure was used for the preparation of **2NTf<sub>2</sub>** and **2PF<sub>6</sub>** from **2Br**. For the preparation of **2PF<sub>6</sub>**,  $\text{LiPF}_6$  was used as the salt.

**Anion exchange via  $\text{AgNTf}_2$ :** **2I** being not soluble in water, a mixture of methanol (MeOH) and water (70-30) was used to obtain a stable solution of **2I**. The addition of a  $\text{LiNTf}_2$  solution (MeOH +  $\text{H}_2\text{O}$ ) to the solution of **2I** (following a similar procedure to that described for **2Cl** and **2Br**) led to quick precipitation of the product. In this case, XPS analysis revealed that only 20% of iodide was replaced by  $\text{NTf}_2$ . Therefore, the anion exchange procedure was modified to achieve complete exchange. In a typical procedure, 30 mg of **2I** was dissolved in 15 ml of methanol. 200 mg  $\text{AgNTf}_2$  pre-dissolved in 15 ml of methanol was slowly added to the solution and stirred overnight. All the operation was carried out under an argon atmosphere. The mixture was centrifuged at 8000 rpm for 15 minutes to separate  $\text{AgI}$  (light yellow precipitate). The clear black solution obtained was reduced to ~5 ml by evaporation. Excess of  $\text{AgNTf}_2$  was removed by dialysis of the solution in distilled water. After 24 hours, the resulting black precipitate was collected and washed several times with distilled water. It is worth mentioning here that, during dialysis,  $\text{Ru}(0)$  may get converted to its oxide and can adversely affect the catalytic activity of NPs. To reduce the amount of Ru oxide in the final sample, dialyzed NPs were subjected to an additional reduction step. In this step, a 5 ml solution of dialyzed NP (in methanol) was stirred for 16 hrs at 50 °C under 5 bars of hydrogen pressure. Then it was dried under vacuum at 35 °C till a constant weight was obtained.

**2Br<sup>†</sup>** was obtained by anion exchange between **2NTf<sub>2</sub>** and an excess of  $\text{LiBr}$ . In this case, **2NTf<sub>2</sub>** was dissolved in acetone (1.5 mg/ml) and  $\text{LiBr}$  (4 molar equivalent) pre-dissolved in acetone was added dropwise under stirring. The mixture was stirred for 16 hours to ensure a complete exchange of  $\text{NTf}_2^-$  with  $\text{Br}^-$ . Upon anion exchange, **2Br<sup>†</sup>** precipitated out of the solution, after being washed with acetone and centrifuged twice to remove excess  $\text{LiBr}$ , **2Br<sup>†</sup>** was dried under vacuum at 35 °C till a constant weight was obtained.

Anions \ Solvents	2Cl	2Br	2I	2NTf <sub>2</sub>	2Br <sup>†</sup>	PVP
H <sub>2</sub> O	✓	✓			✓	✓
Methanol	✓	✓	✓	✓	✓	✓
C <sub>3</sub> H <sub>8</sub> O	✓	✓	✓		✓	
CHCl <sub>3</sub>	✓	✓	✓		✓	✓
CH <sub>2</sub> Cl <sub>2</sub>	✓	✓	✓		✓	✓
THF				✓		
C <sub>4</sub> H <sub>8</sub> O <sub>2</sub>				✓*		

(✓) indicates solubility of catalyst in the respective solvent.

\***2NTf<sub>2</sub>** is partially soluble in ethyl acetate.

†**2PF<sub>6</sub>** is not soluble at room temperature but forms a sticky substance at high temperature (around 100 °C)

### 3. Ru content determination by TGA

Ru content of all NP samples was determined by thermogravimetric analysis (TGA) using a TGA Q-500 from TA instruments. A typical TGA curve of **PIL(Cl)** (a), **2Cl** (b), and **2Br** (c) are shown in Figure S4. Initially, samples were heated in a nitrogen environment till 600 °C and subsequently in the air till 750 °C. Residual weight obtained after the introduction of air was considered as the Ru content.

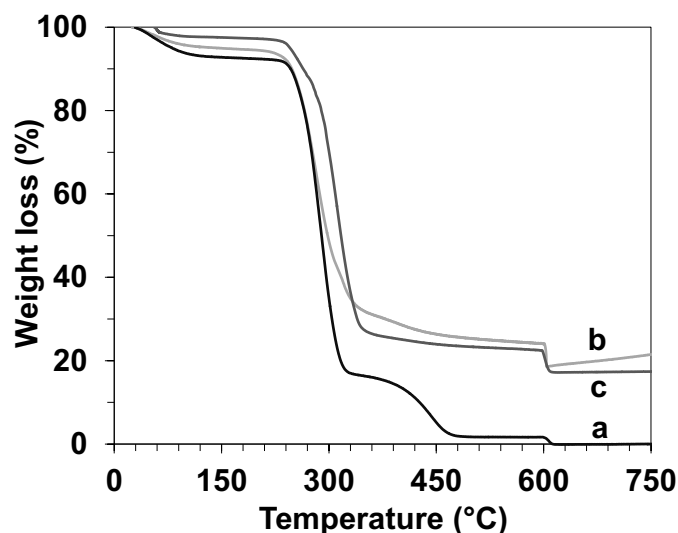


**Figure S4.** TGA curve of (a) **PIL(Cl)** (b) **2Cl** and (c) **2Br** showing weight loss with temperature. Residual weight after 600 °C was considered as the Ru content of the samples.

**Table S3.** Ru content of NP samples determined by TGA.

Entries	Sample	Ru content (%)
1	1Cl	9.8
2	2Cl	18.1
3	3Cl	29
4	2Br	17.1
5	2I	11.2
6*	IL(Cl)@RuNP	13.9
7 <sup>#</sup>	PVP@RuNP	10.1
8	2NTf <sub>2</sub>	9.3
9 <sup>†</sup>	2NTf <sub>2</sub>	5.7
10	2Br <sup>†</sup>	17.6

\*Ru NPs obtained by using 1-Butyl-3-ethylimidazolium bromide (IL).

<sup>#</sup>PVP stabilized Ru NPs.

<sup>†</sup>Obtained from 2I via anion exchange with AgNTf<sub>2</sub>.

## 4. TEM analysis of Ru nanoparticles

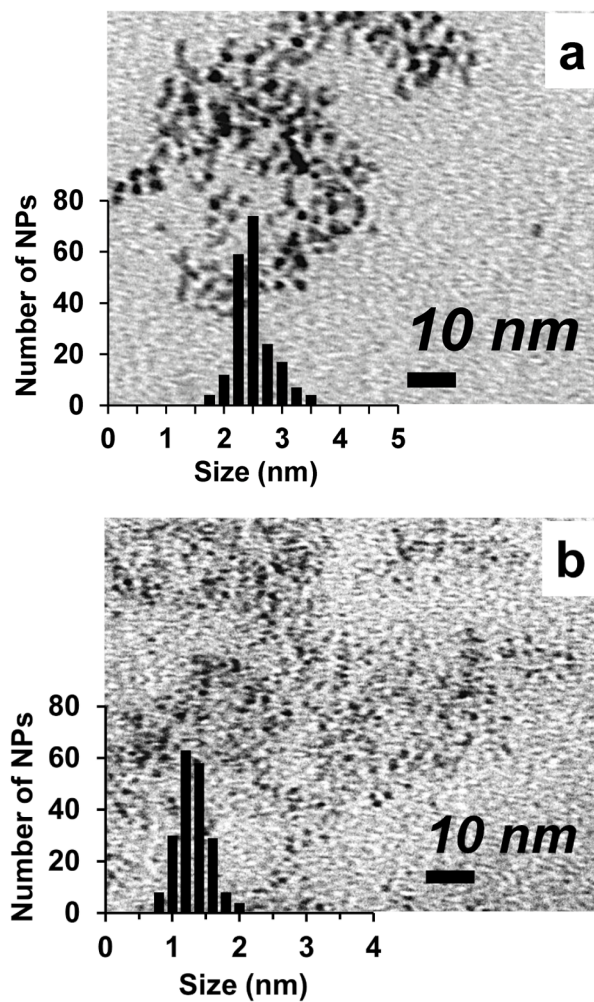


Figure S5. TEM images of (a) 2Br and (b) 2I.

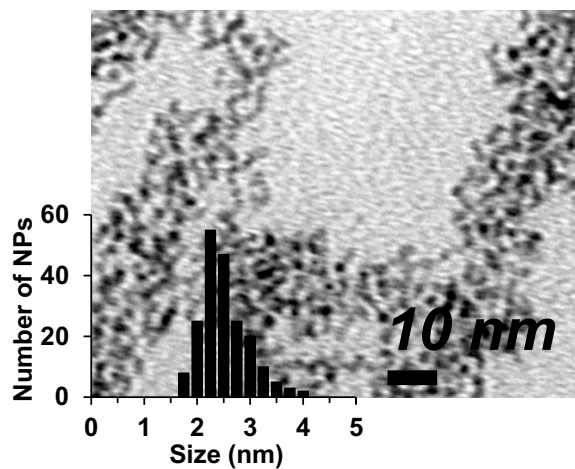
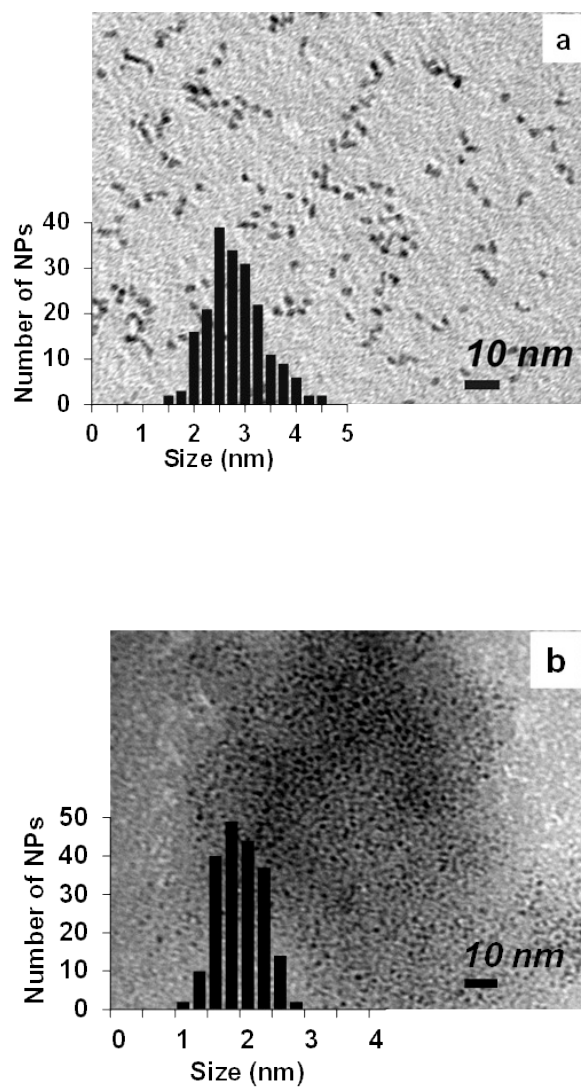
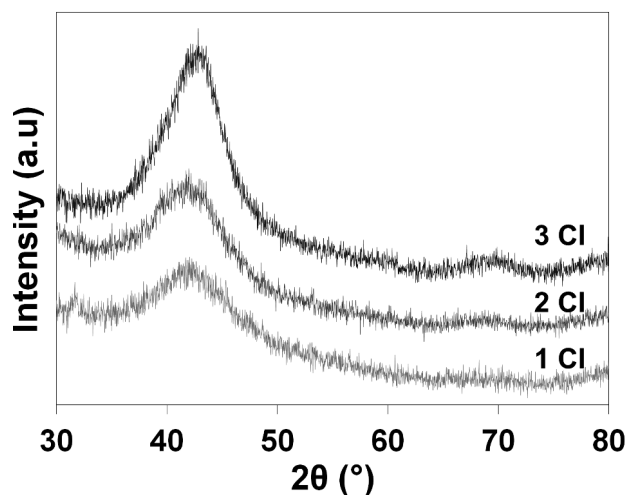


Figure S6. (a) TEM images of 2NTf<sub>2</sub> resulting from the anion exchange between 2Br and LiNTf<sub>2</sub>. No change in the size of the particles was observed after anion exchange.



**Figure S7.** TEM images of Ru NPs synthesized using (a) Poly(vinylpyrrolidone) (PVP@RuNP) and (b) 1-Butyl-3-ethylimidazolium bromide (IL@RuNP). Note: 0.1 molar equivalents of  $\text{RuCl}_3 \cdot \text{XH}_2\text{O}$  was used with respect to monomeric unit.

## 5. X-ray diffraction (XRD) patterns of Ru NPs



**Figure S8.** Powder XRD pattern of Ru NPs synthesized using PIL(Cl). The peak corresponding to Ru (101) plane can be seen at  $43^\circ$  ( $2\theta$ ).<sup>9,10</sup> With an increase in precursor ( $\text{RuCl}_3$ ) loading from 1Cl to 3Cl, the sharpening of the peak for the 101 plane is in agreement with an increase in NP size.

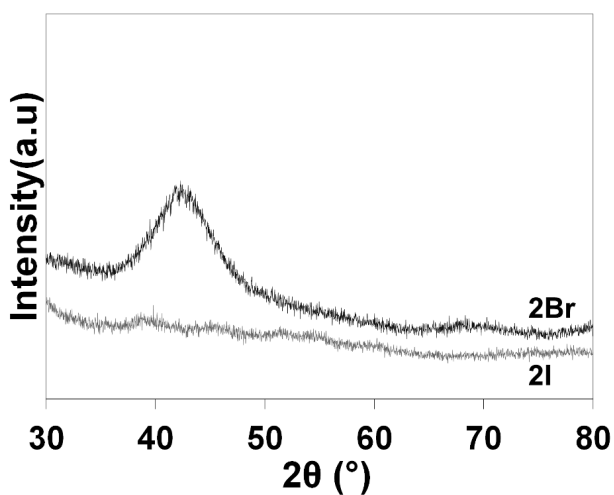


**Figure S9.** Powder XRD pattern of 2Br and 2I. In the case of 2I (1.2 nm by TEM, Figure S3), the sizes of the crystalline domains are too small to observe a signal.<sup>11</sup>

**Table S4.** Size of different Ru NPs determined by TEM and XRD analysis.

Sample	NP size (nm) by TEM	NP size (nm) by XRD (Debye-Scherrer relation)
1Cl	$1.47 \pm 0.25$	1.10
2Cl	$2.55 \pm 0.38$	1.26
3Cl	$2.65 \pm 0.75$	1.39
2Br	$2.30 \pm 0.30$	1.33
2I	$1.21 \pm 0.24$	-
IL(Cl)@RuNP*	$1.8 \pm 0.33$	-
PVP@RuNP	$2.70 \pm 0.56$	-
2NTf <sub>2</sub>	$2.40 \pm 0.45$	-
2Br <sup>l</sup>	$2.35 \pm 0.55$	2.0

\*Nano particles synthesized using 1-Butyl-3-ethylimidazolium bromide.

## 6. $\zeta$ -potentials of Ru NPs

$\zeta$ -potentials of all NPs were measured at 25 °C by Malvern Zetasizer ZS.  $\zeta$ -potentials were measured in water for **1-3Cl**, **2Br**, and **PVP@RuNP** (Table S5) and in MeOH for **1-3Cl**, **2Br**, **2I**, **2NTf<sub>2</sub>** and **PVP@RuNPs** (Table S6).

**Table S5.**  $\zeta$ -potential of PILs and PVP stabilized Ru NPs in water.

Sample	$\zeta$ -potentials in water (mV)
1Cl	55.5 ± 2.4
2Cl	49.4 ± 0.5
3Cl	34.9 ± 1.6
2Br	58.3 ± 1.1
PVP@RuNP	8.2 ± 0.4

Note:  $\zeta$ -potential was measured at 25 °C.

**Table S6.**  $\zeta$ -potentials of PILs and PVP stabilized Ru NPs in methanol.

Sample	$\zeta$ -potential (mV)
1Cl	38.0 ± 1.4
2Cl	38.0 ± 0.8
3Cl	37.2 ± 1.3
2Br	40.0 ± 1.1
2NTf <sub>2</sub>	41.8 ± 1.1
2I	40.1 ± 1.1
PVP@RuNP	2.6 ± 0.3

Note:  $\zeta$ -potential was measured at 25 °C.

## 7. XPS analysis

X-ray photoelectron spectroscopy (XPS) analysis was carried out on PIL(X) and PIL(X)@RuNPs to study the nature of the interaction between PILs and RuNPs. K-Alpha X-ray Photoelectron Spectrometer from Thermo Fisher Scientific equipped with monochromatized AlK $\alpha$  source ( $h\nu=1486.6$  eV) was used for surface analysis. The full spectra (0-1350eV) and high-resolution spectra were recorded with a constant pass energy of 200 eV and 40 eV respectively. Ar<sup>+</sup> sputtering was used for depth profiles. High-resolution spectra were processed and fitted with AVANTAGE software from Thermo Fisher Scientific. All the scans were corrected considering C(1s) as the reference (285.0 eV).<sup>12,13</sup>

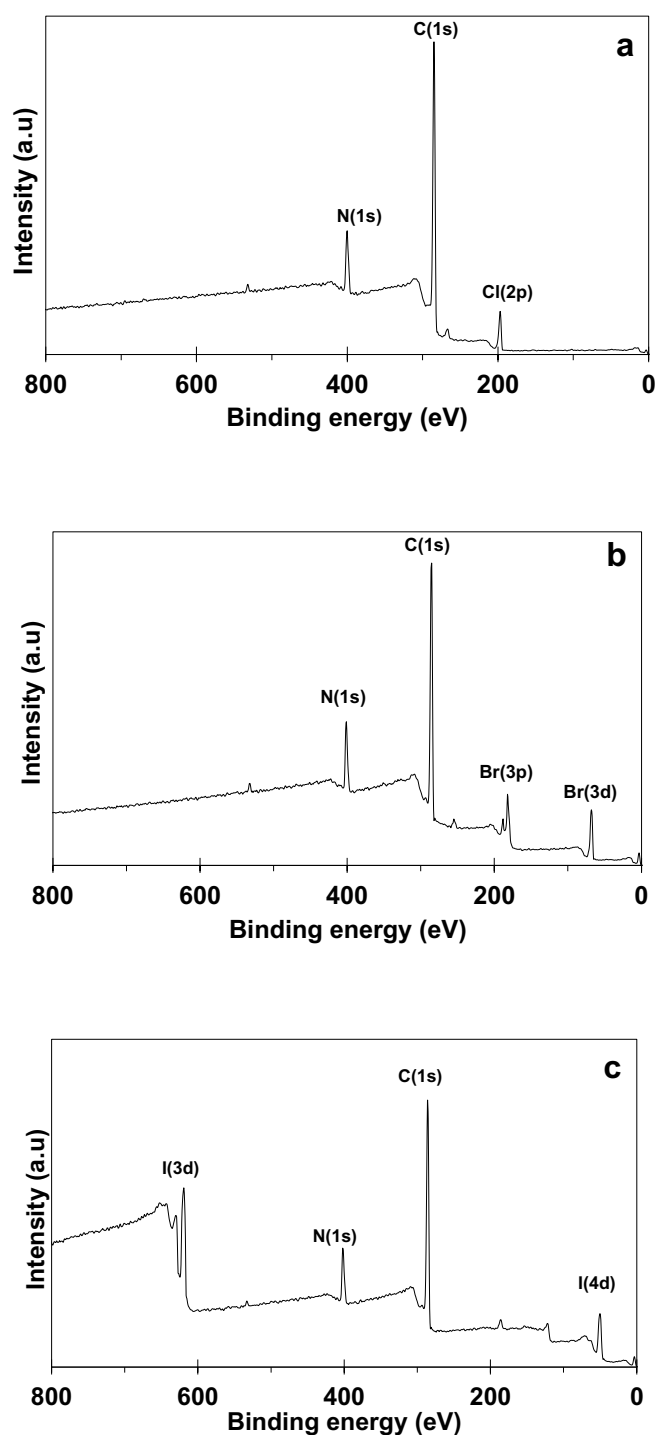


Figure S10. XPS survey scan of (a) PIL(Cl), (b) PIL(Br) and (c) PIL(I).

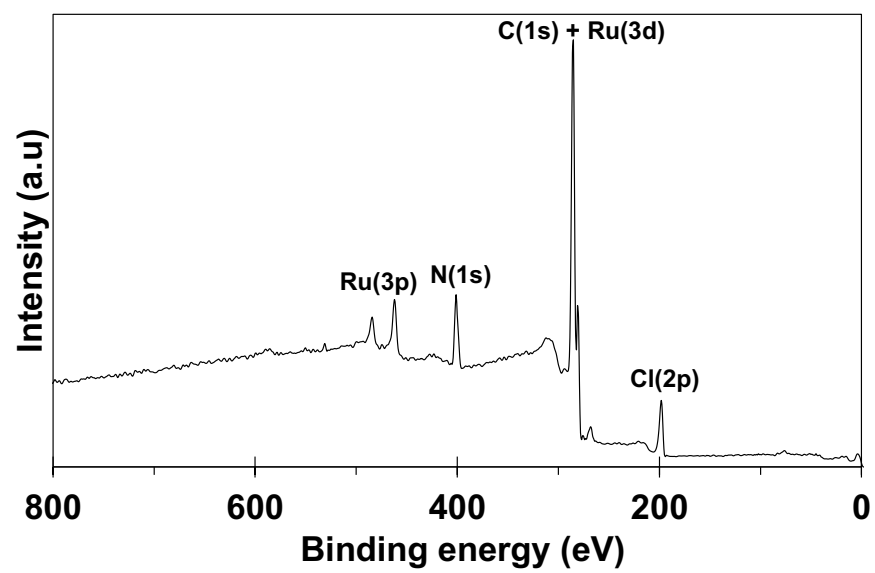


Figure S11. XPS survey scan of PIL(Cl) stabilized Ru NP (2Cl).

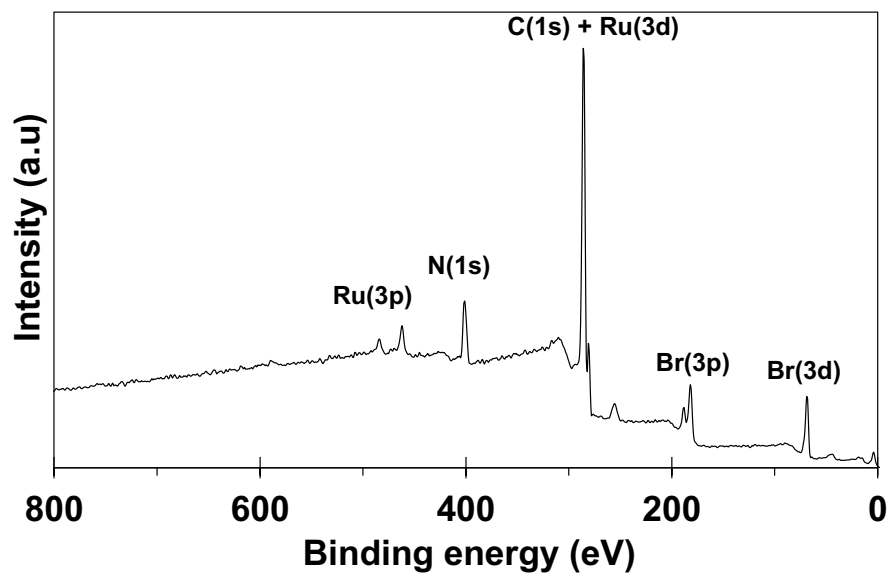
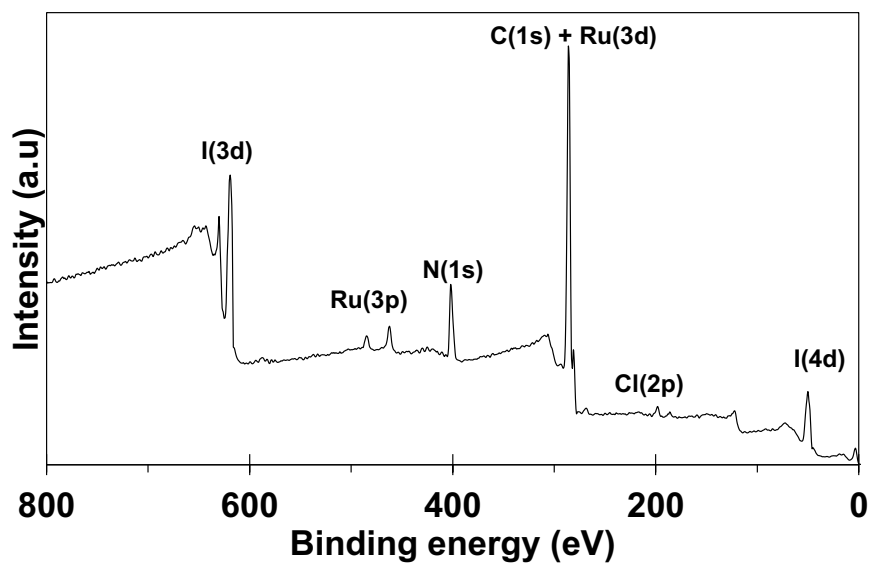
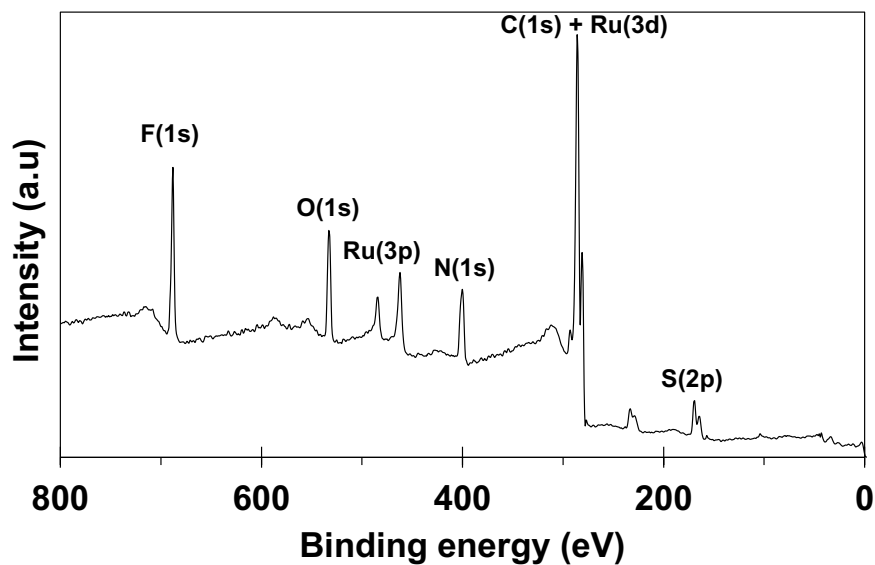


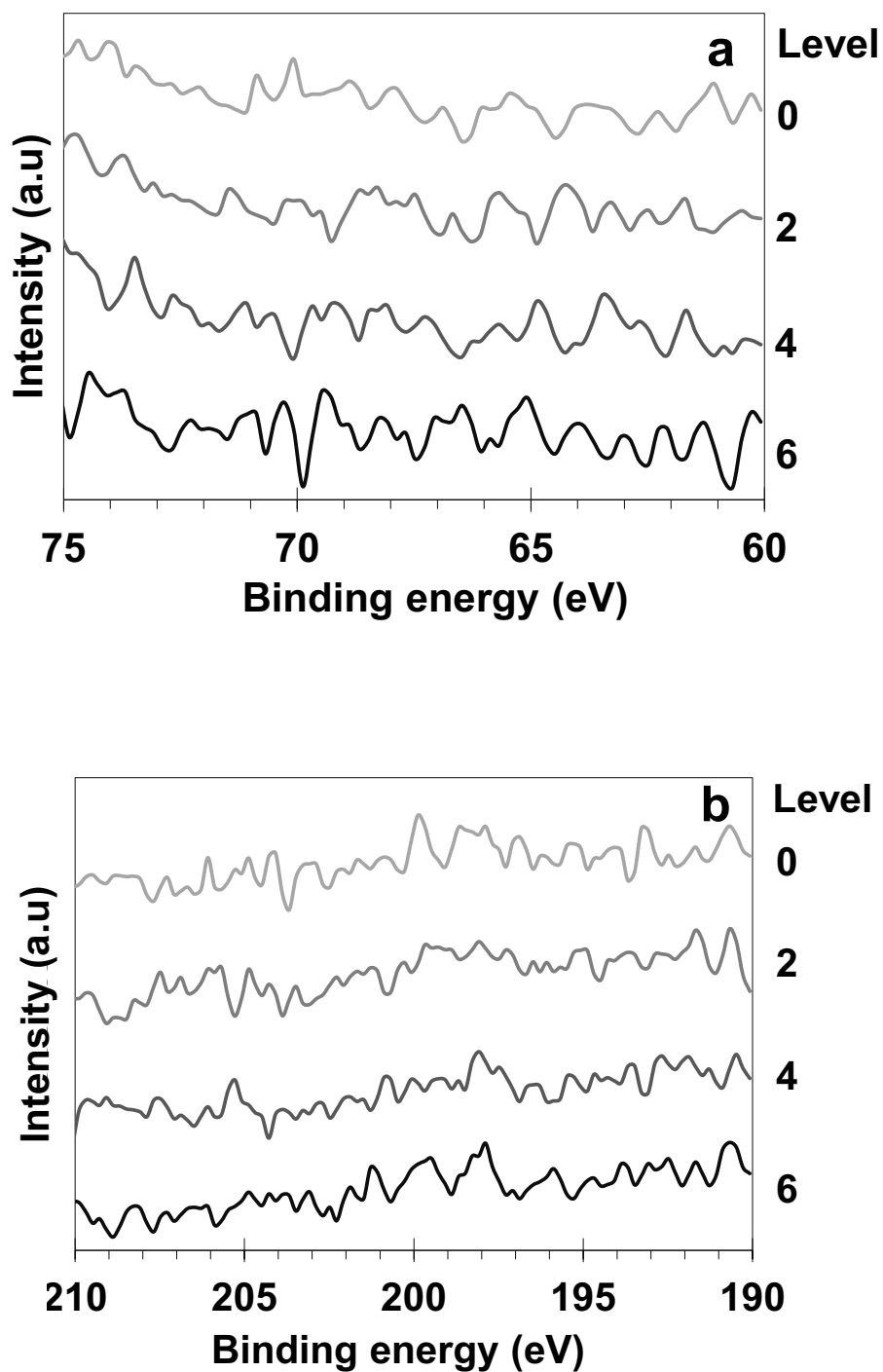
Figure S12. XPS survey scan of PIL(Br) stabilized Ru NP (2Br).



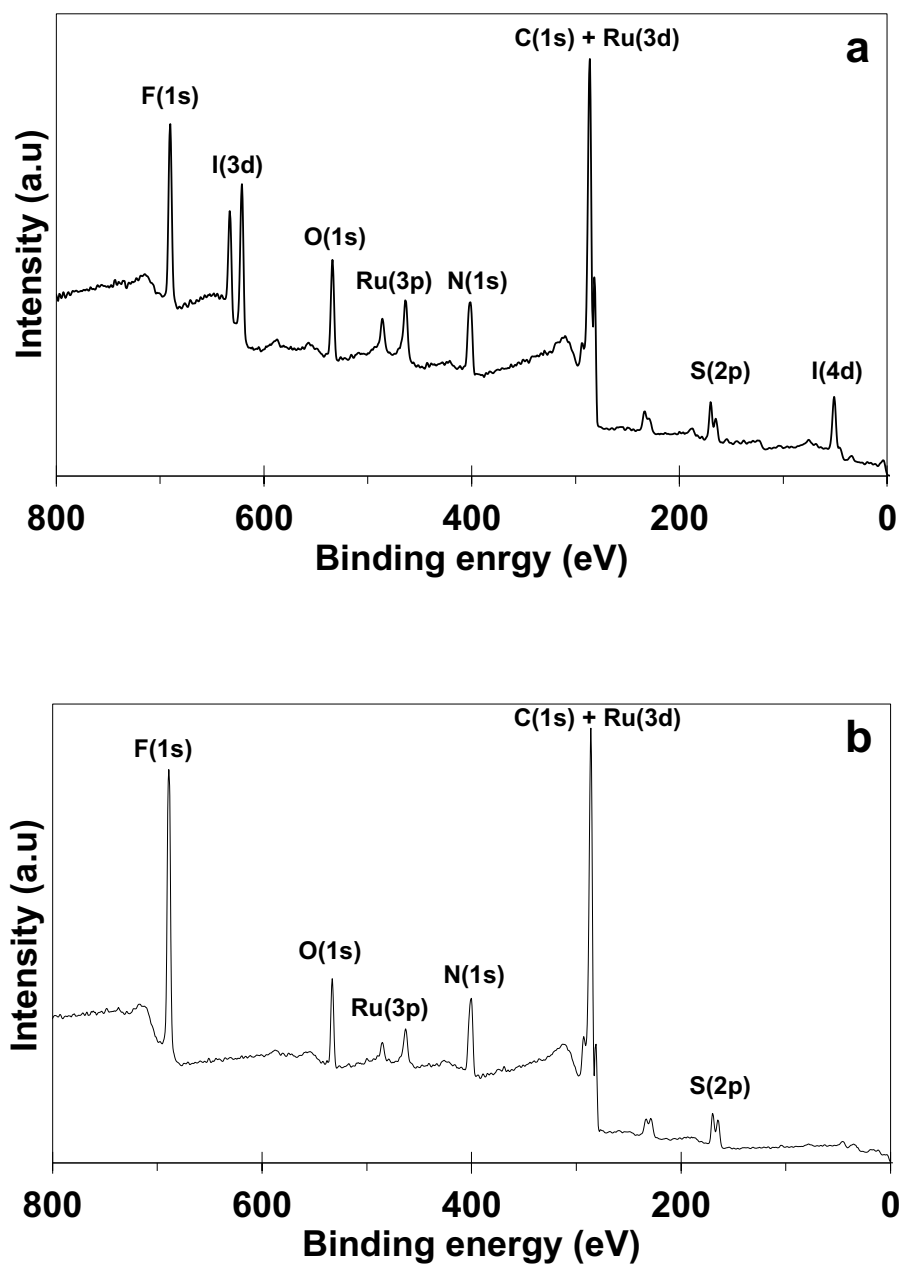
**Figure S13.** XPS survey scan of **2I**. The presence of Cl(2p) peak can be attributed to the exchange of  $\text{I}^-$  by  $\text{Cl}^-$  (2%) during NP synthesis using  $\text{RuCl}_3$  as a precursor.



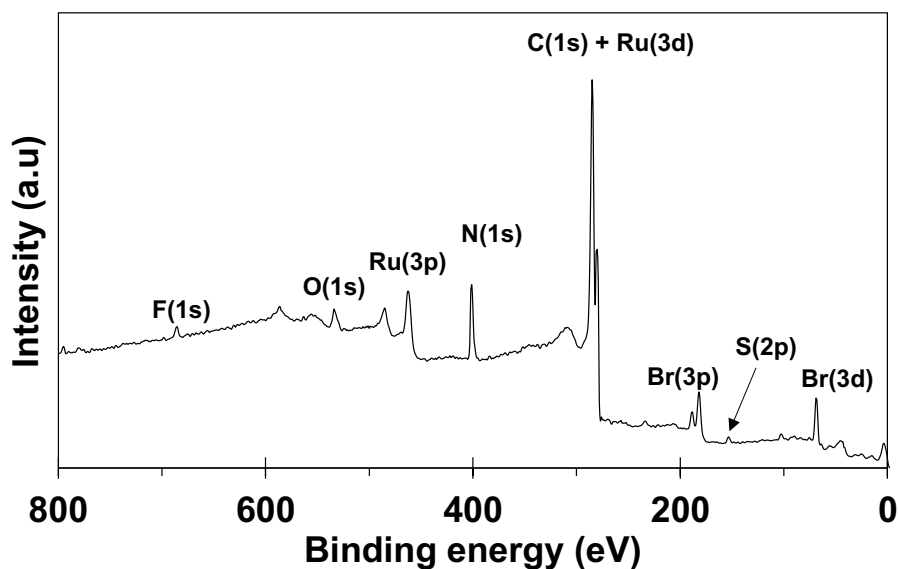
**Figure S14.** XPS survey scan of **2NTf<sub>2</sub>** NPs obtained after anion exchange between **2Br** and  $\text{LiNTf}_2$ . The absence of any characteristic peak for Br is a sign of the complete exchange of  $\text{Br}^-$  by  $\text{NTf}_2^-$ .



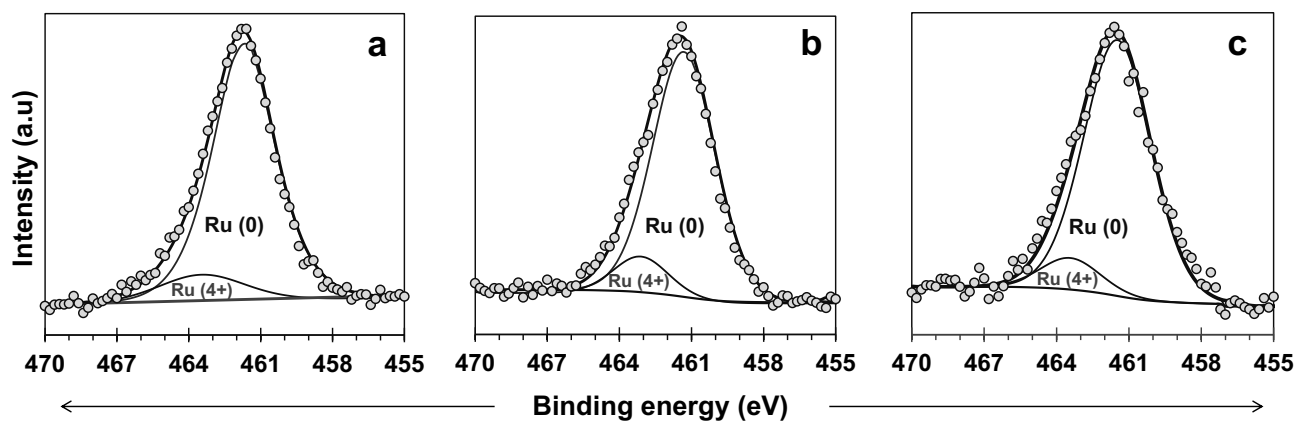
**Figure S15.** High-resolution XPS scan of (a) Br(3d) region of  $2\text{NTf}_2$  at different depths. The absence of Br(3d) peak indicates the complete replacement of  $\text{Br}^-$  by  $\text{NTf}_2^-$ . (b) Cl 2p region scan of  $2\text{NTf}_2$  (prepared from  $2\text{Cl}$ ) at different depths. The absence of Cl 2p peak indicates complete replacement of  $\text{Cl}^-$  by  $\text{NTf}_2^-$  during anion exchange



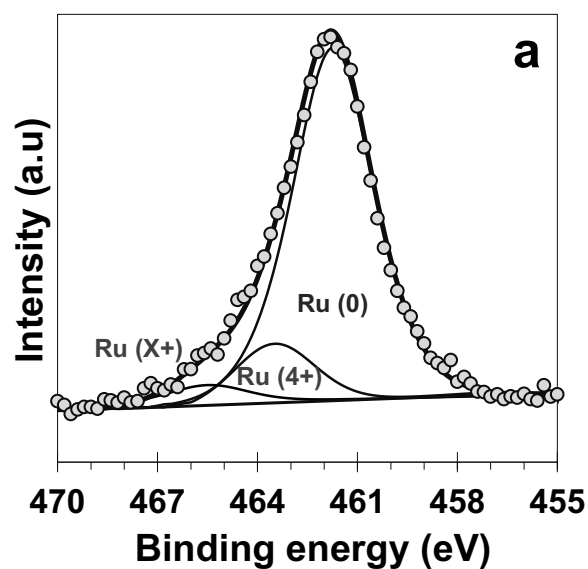
**Figure S16.** (a) XPS survey scan of NPs obtained after anion exchange between **2I** and  $\text{LiNTf}_2$ . A strong peak of I(3d) at 614 eV indicates the partial replacement of  $\text{I}^-$  by  $\text{NTf}_2^-$  (~21%). (b) XPS survey scan of NPs obtained after anion exchange between **2I** via  $\text{AgNTf}_2$ , absence of characteristic peak of iodide indicates successful exchange of  $\text{I}^-$  by  $\text{NTf}_2^-$ .



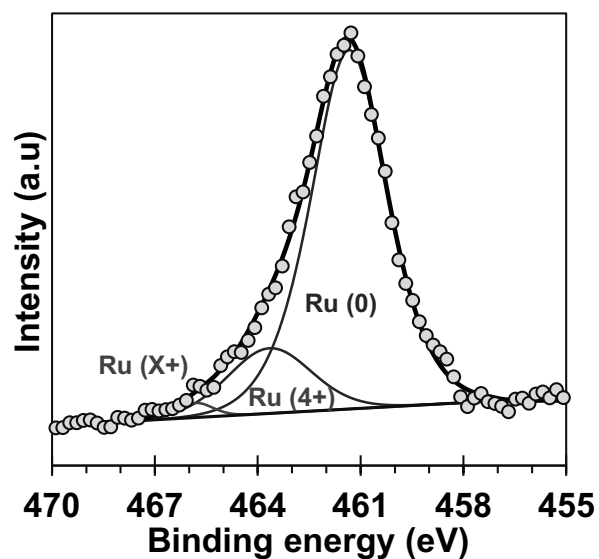
**Figure S17.** XPS survey scan of **2BrI** resulting from the anion exchange reaction between **2NTf<sub>2</sub>** and LiBr. F(1s) and S(2p) peaks in the scan is due to some residual (~8 %) NTf<sub>2</sub><sup>-</sup> in the sample.



**Figure S18.** High resolution Ru(3p) scan of (a) **2ClI**, (b) **2BrI** and (c) **2I**. Deconvolution of Ru(3p) shows different oxidation states of Ru present in PILs stabilized NPs. From the figures, it is evident that NPs are mainly composed of Ru(0) (at 461.4 eV) and a small proportion of Ru(4+) towards higher BE (463.4 eV).<sup>14-16</sup>



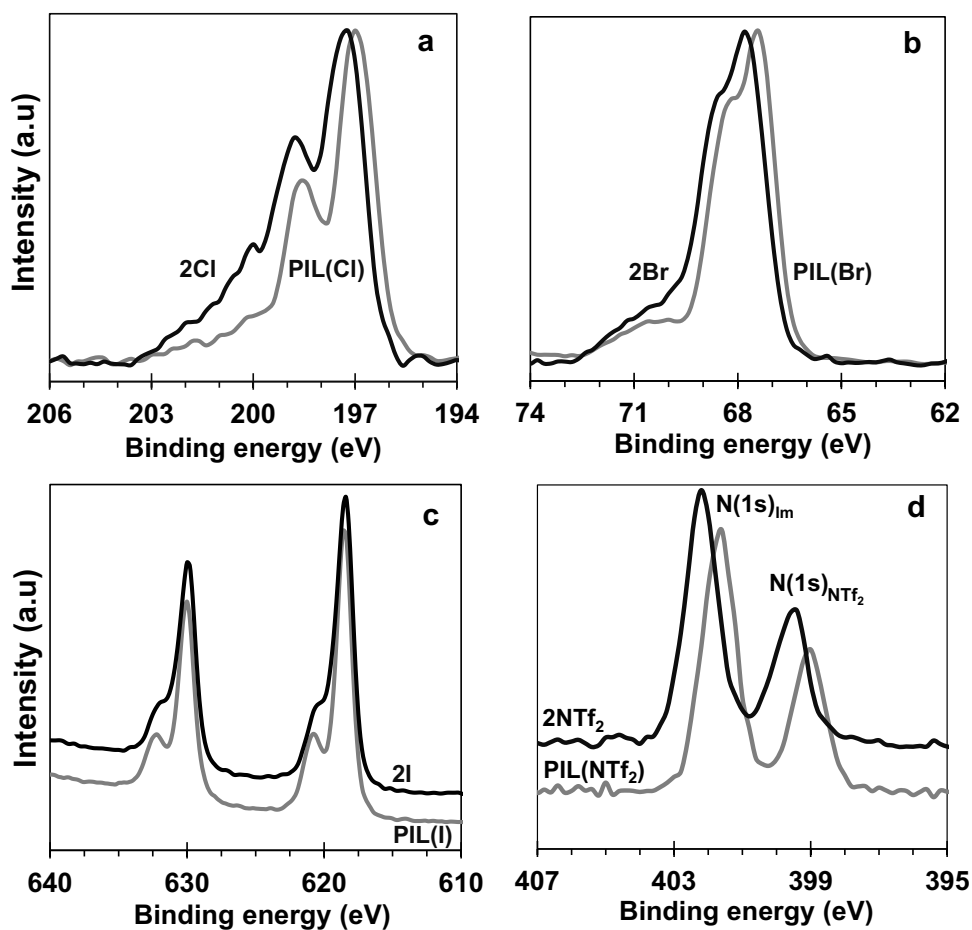
**Figure S19.** High-resolution Ru(3p) scan showing different oxidation states of Ru present in 2NTf<sub>2</sub>. An additional high binding energy component assigned to Ru(X<sup>+</sup>) (at 465.9 eV) was detected,<sup>15,17</sup> which results from the exposure to air during purification after anion exchange.



**Figure S20.** High-resolution scan of Ru(3p) showing different oxidation states of Ru present in 2Br<sup>+</sup>.

**Table S7.** Different oxidation states of Ru and their proportion in NPs determined by deconvolution of Ru(3p) scan.

Entry	Sample	Position of peaks and Ru(0) composition		
		Ru(0) [Area %]	Ru(4+) [Area %]	Ru(X+) [Area %]
1	2Cl	461.3 [88.4]	463.4 [11.6]	-
2	2Br	461.4 [91.5]	463.4 [8.5]	-
3	2NTf <sub>2</sub>	461.4 [85.1]	463.4 [10.3]	465.9 [4.6]
4	2Br'	461.4 [82.7]	463.4 [15.7]	465.9 [1.6]
5	2I	461.4 [90.3]	463.4 [9.7]	-

**Figure S21.** Overlay of high resolution XPS scan of (a) Cl(2p) region of PIL(Cl) and 2Cl, (b) Br(3d) region of PIL(Br) and 2Br, (c) I(3d) region of PIL(I) and 2I and of (d) N(1s)<sub>Im</sub> and N(1s)<sub>NTf<sub>2</sub></sub> in PIL(NTf<sub>2</sub>) and 2NTf<sub>2</sub>.

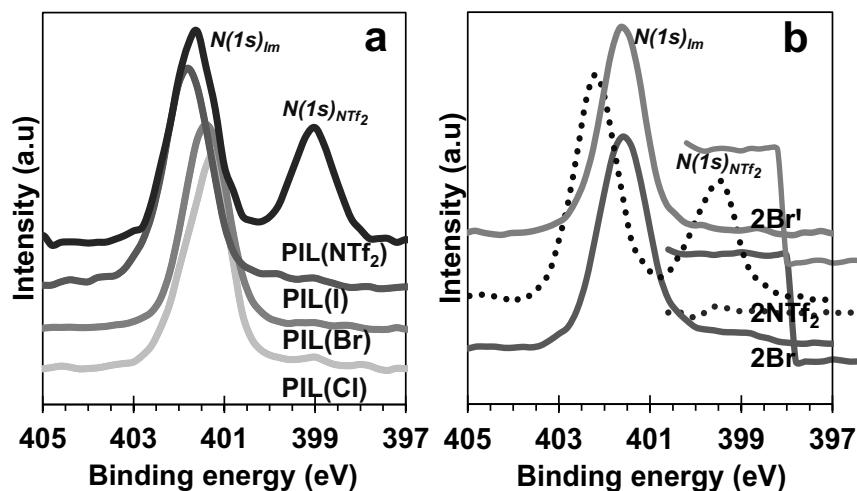


**Figure S22.** High-resolution XPS scan in N(1s) region of (a) PILs showing the shift in the binding of imidazolium N(1s) in presence of different anions (b) showing the change in the BE of N(1s)Im before anion exchange (**2Br**), after Br/NTf<sub>2</sub> anion exchange (**2NTf<sub>2</sub>**) and after NTf<sub>2</sub>/Br anion exchange (**2Br'**). The same BE observed for N(1s)Im in both **2Br** and **2Br'** suggest that a similar environment around the surface of Ru NPs (to that of the starting **2Br**) has been recovered after two successive anion exchange reactions.

The signals corresponding to the binding energy (BE) of all halogen atoms (Cl, Br, I) appear as (non-symmetrical) doublets because of spin-orbit couplings. The value of the BE of the anion was given according to the most intense component of the doublet that appears at the lowest BE (Table S8). All halogens feature both in the “free” PIL(X) (X= Cl, Br, I) and in the corresponding PIL(X)@RuNPs (**2Cl**, **2Br**, **2I**) a minor signal that appears at relatively higher BE compared to the most intense signals. Although it is difficult to attribute a specific environment to each signal, we may hypothesize that the difference in BE between the major and minor signals could be related to the number or nature of interactions between the different anions and the C<sub>2</sub>-H, C<sub>4</sub>-H, and C<sub>5</sub>-H by H-bonding.<sup>18</sup> The major signal appearing at the lowest BE would then correspond to a situation where the anion is involved in a fewer H-bond (1 or 2) compared to the minor signal at higher BE, which would be involved in multiple H-bonds (2 or more). For simplicity, only discussions about the BE of the major signals and their shifts between the polymer and the corresponding NP have been included in the main text. In the case of the NTf<sub>2</sub> anion, binding to the Ru surface could occur either via the N atom or via the O atoms<sup>18</sup> but XPS analysis does not allow to rule out one of those interactions.

In the case of the iodide anion, the absence of a shift in the BE of I(3p) between PIL(I) and the respective NP (**2I**) suggests that I<sup>-</sup> do not interact significantly with the metal surface. In contrast, the shift of the N(1s) of the imidazolium moieties N(1s)Im toward lower BE observed in the XPS spectrum of **2I** (compared to that observed in PIL(I)) suggests an interaction between the imidazolium cation and the Ru surface. We may hypothesize that the imidazolium cation lies parallel to the surface by analogy with the stabilization of gold NPs in imidazolium-based ILs (see Figure S23).<sup>20</sup> However, the interaction of the imidazolium cation with the Ru surface via the C<sub>4</sub>-H/C<sub>5</sub>-H or via the C<sub>2</sub>-H might also be postulated (Figure S23).<sup>19</sup> As a result of this cation-surface interaction, the surface becomes seriously hindered, which certainly prevents aromatic moieties to adsorb by “ $\pi$ -stacking” onto the flat surface. Nevertheless, this interaction does not prevent the binding of alkenes to the edges or corners of **2I**, which allows unsaturated substrates, such as styrene, to undergo selective hydrogenation of the C=C bond.

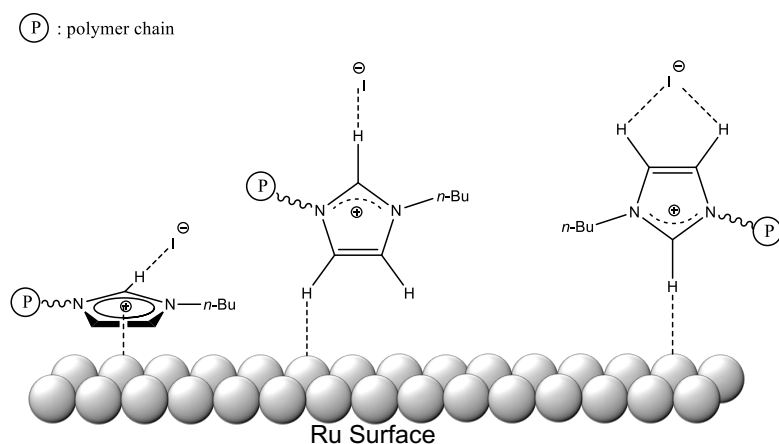


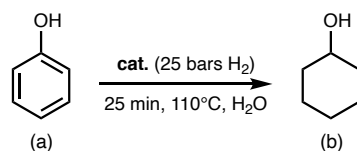
**Figure S23.** Schematic representations of possible interactions between the imidazolium cation and the RuNP surface in the case of **2I**.

**Table S8.** The binding energy of different elements in PIL(X) (X = Cl, Br, I, NTf<sub>2</sub>) and in the corresponding PIL stabilized Ru NPs.

Sample	C(1s)	N(1s) <sub>im</sub>	Anion	Ru
			<b>Cl (2p)</b>	<b>3d</b> <b>3p</b>
PIL(Cl)	285.0	401.2	197.0	-      -
2Cl	285.0	401.6	197.2	280.2      461.4
			<b>Br (3d)</b>	<b>3d</b> <b>3p</b>
PIL(Br)	285.0	401.4	67.4	-      -
2Br	285.0	401.6	67.8	280.4      461.4
			<b>I (3d)</b>	<b>3d</b> <b>3p</b>
PIL(I)	285.0	401.8	618.4	-      -
2I	285.0	401.6	618.4	280.4      461.6
			<b>NTf<sub>2</sub> (N1s)</b>	<b>3d</b> <b>3p</b>
PIL(NTf <sub>2</sub> )	285.0	401.6	399.0 (N)	-      -
2NTf <sub>2</sub>	285.0	402.2	399.4 (N)	280.8      461.8

## 8. Catalytic activity

## (a) Hydrogenation of phenol by Ru NPs

**Table S9.** Hydrogenation of Phenol in water by PILs, ionic liquid and PVP stabilized Ru NPs.

Entries	Catalyst	Conversion (%)	Selectivity (b %)	Remark
1	2Br	100	100	-
2	2Cl	100	100	The catalyst was recycled (fig. S24)
3	IL(Cl)@RuNPs	100	100	Formation of bulk metal
4	PVP@Ru	100	100	Aggregation of NPs

Hydrogenation were performed at 110 °C for 25 min, using 25 bars of H<sub>2</sub>, 0.166 mol.% of Ru and water as solvent. Conversion was determined by determined by <sup>1</sup>H NMR.

## (b) Recycling of PIL stabilized Ru NP (2Cl) during hydrogenation of phenol in water

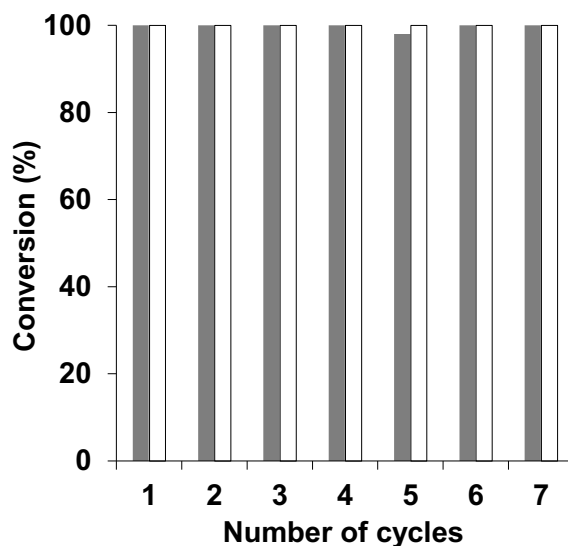


**Figure S24.** Activity and selectivity of 2Cl during recycling. Phenol was used as a substrate at 0.166 mol% Ru loading, 25 bars of H<sub>2</sub> and 110 °C. Hydrogenation time was kept 25 minutes for every cycle. Grey bars represent phenol conversion and the white bar indicates cyclohexanol selectivity. At every cycle, complete hydrogenation of phenol to cyclohexanol indicates remarkable stability of PIL stabilized Ru nanoparticles.

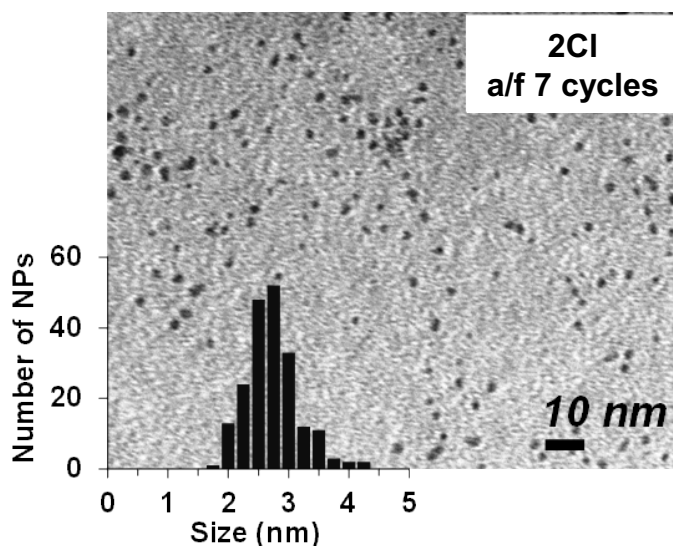


**Figure S25.** TEM image of 2Cl after 7th hydrogenation cycle. From the particle size and distribution, it can be confirmed that PILs stabilized RuNPs do not agglomerate even after multiple hydrogenation cycles under the hydrogenation conditions (Phenol hydrogenation at 110 °C for 25 min, using 25 bar of H<sub>2</sub> and 0.166 mol.% of Ru).

**(c) Catalyst poisoning by CS<sub>2</sub>**

To confirm the heterogeneous nature of Ru NP catalysts, CS<sub>2</sub> poisoning test was carried out on 2Cl during hydrogenation of phenol in water.<sup>21, 22</sup> Hydrogenation was started as per the procedure described in section 2d. The reaction temperature was maintained at 30 °C. After the desired time, the reactor was depressurized to collect the sample for determining phenol conversion. At this time, CS<sub>2</sub> dissolved in THF was injected (0.5 molar equivalents relative to Ru) into the reactor followed by re-pressurization with H<sub>2</sub>. Then the reactor was immersed in the preheated oil bath (30 °C) to start the hydrogenation. After 4 hours, the reactor was cooled down and depressurized to stop the reaction. The product was extracted with diethyl ether and taken for <sup>1</sup>H NMR analysis upon evaporating diethyl ether (no vacuum). GC-MS analysis was also carried out to confirm conversions (Figure S26).

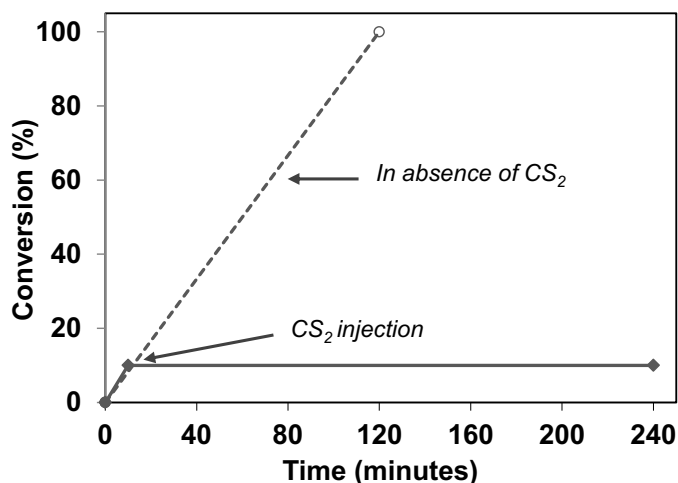


**Figure S26.** Plot showing phenol conversion in the absence (dotted line) and presence (solid line) of CS<sub>2</sub>. After the addition of CS<sub>2</sub> (at 10 min), conversion remained unchanged which is the characteristic of heterogeneous hydrogenation. Hydrogenation was carried out at 0.166 mol% Ru loading, 25 bar H<sub>2</sub>, 30 °C.

(d) Toluene hydrogenation using 2NTf<sub>2</sub>**Table S10.** Influence of solvent on the catalytic activity of 2NTf<sub>2</sub> during hydrogenation of Toluene.

Entries	Ru NP	Solvent	Conversion of toluene (%)
1	2NTf <sub>2</sub>	MeOH	70
2	2NTf <sub>2</sub>	THF	100
3*	2NTf <sub>2</sub>	Ethyl Acetate	65

Hydrogenation was performed at 110 °C for 60 min in the required quantity of solvent, using 25 bars of H<sub>2</sub> and 0.33 mol.% of Ru. In all cases, conversion was determined by GC-MS.  
\*2NTf<sub>2</sub> is partially soluble in Ethyl acetate.

## 9. Activity switching of Ru NPs

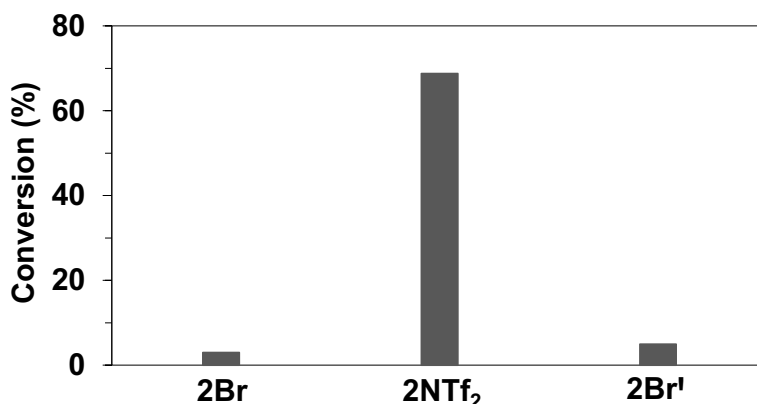


**Figure S27.** Demonstrating activity switching of PIL(Br) stabilized Ru NPs (2Br) by simple anion exchange route. All hydrogenation experiments were carried out using toluene as a substrate at 0.33% Ru loading, 25 bars H<sub>2</sub>, and 100 °C for 60 mins.

## 10. References

1. R. Marcilla, J. B. Alberto, J. Rodriguez, J. A. Pomposo and D. Mecerreyes, *J. Polym. Sci., Part A: Polym. Chem.*, 2004, **42**, 208-212.
2. Y. Rong, Z. Ku, M. Xu, L. Liu, M. Hu, Y. Yang, J. Chen, A. Mei, T. Liu and H. Han, *RSC Adv.*, 2014, **4**, 9271-9274.
3. R. Thenarukandiyil, H. Thrikkykkal and J. Choudhury, *Organometallics*, 2016, **35**, 3007-3013.
4. H. He, M. Zhong, B. Adzima, D. Luebke, H. Nulwala and K. Matyjaszewski, *J. Am. Chem. Soc.*, 2013, **135**, 4227-4230.
5. M. Ohtaki, M. Komiyama, H. Hirai and N. Toshima, *Macromolecules*, 1991, **24**, 5567-5572.
6. L. S. Sarma, C.-H. Chen, S. M. S. Kumar, G.-R. Wang, S.-C. Yen, D.-G. Liu, H.-S. Sheu, K.-L. Yu, M.-T. Tang, J.-F. Lee, C. Bock, K.-H. Chen, B.-J. Hwang, *Langmuir*, 2007, **23**, 5802-5809.
7. X. Yan, H. Liu and K. Y. Liew, *J. Mater. Chem.*, 2001, **11**, 3387-3391.
8. H. Erdoğan, Ö. Metin and S. Özkar, *Catal. Today*, 2011, **170**, 93-98.
9. M. Fang, N. Machalaba and R. A. Sanchez-Delgado, *Dalton Trans.*, 2011, **40**, 10621-10632.
10. H. Jang, S.-H. Kim, D. Lee, S. E. Shim, S.-H. Baek, B. S. Kim and T. S. Chang, *J. Mol. Catal. A: Chem.*, 2013, **380**, 57-60.
11. S. Mourdikoudis, R. M. Pallares, Nguyen T. K. Thanh, *Nanoscale*, 2018, **10**, 12871-12934.
12. N. Chakroune, G. Viau, S. Ammar, L. Poul, D. Veautier, M. M. Chehimi, C. Mangeney, F. Villain, F. Fiévet, *Langmuir*, 2005, **21**, 6788-6796.
13. T. Cremer, C. Kolbeck, K. R. J. Lovelock, N. Paape, R. Wölfel, P. S. Schulz, P. Wasserscheid, H. Weber, J. Thar, B. Kirchner, F. Maier and H.-P. Steinrück, *Chem. Eur. J.*, 2010, **16**, 9018-9033.

## SUPPORTING INFORMATION

---

14. Yang, J., Lee, J. Y., Deivaraj, T. C., Too, H.-P. Preparation and characterization of positively charged ruthenium nanoparticles. *J. Colloid Interface Sci.* **271**, 308-312.
15. M. Zawadzki and J. Okal, *Mater. Res. Bull.*, 2008, **43**, 3111-3121.
16. J. L. Gómez de la Fuente, M. V. Martínez-Huerta, S. Rojas, P. Hernández-Fernández, P. Terreros, J. L. G. Fierro and M. A. Peña, *Appl. Catal., B: Environmental*, 2009, **88**, 505-514.
17. K. Qadir, S. H. Joo, B. S. Mun, D. R. Butcher, J. R. Renzas, F. Aksoy, Z. Liu, G. A. Somorjai and J. Y. Park, *Nano Lett.*, 2012, **12**, 5761-5768.
18. A. Elaiwi, P. B. Hitchcock, K. R. Seddon, N. Srinivasan, Y.-M. Tan, T. Welton and J. A. Zora, *J. Chem. Soc. Dalton Trans.*, 1995, 3467-3472.
19. A. S. Pensado and A. A. H. Pádua, *Angew. Chem. Int. Ed.*, 2011, **50**, 8683-8687.
20. H. S. Schrekker, M. A. Gelesky, M. P. Stracke, C. M. L. Schrekker, G. Machado, S. R. Teixeira, J. C. Rubim and J. Dupont, *J. Colloid Interface Sci.*, 2007, **316**, 189-195.
21. L. M. Rossi and G. Machado, *J. Mol. Catal. A: Chem.*, 2009, **298**, 69-73.
22. C. Vollmer, E. Redel, K. Abu-Shandi, R. Thomann, H. Manyar, C. Hardacre and C. Janiak, *Chem. Eur. J.*, 2010, **16**, 3849-3858.